Research Article

The Numerical Study Of Natural Convection Heat Transfer In A Partially Opened Square Cavity With Internal Heat Source

J.Supraja[1*], G.S.S. Raju[2]
[1]Research Scholar, Department of Mathematics, JNTUA, Ananthapuramu, AP, India
shupraja32@gmail.com
[2]Professor, Department of Mathematics JNTUP, Pulivendula, YSR Kadapa Dist., AP, India
rajugss@yahoo.com

Article History: Received: 11 January 2021; Revised: 12 February 2021; Accepted: 27 March 2021; Published online: 28 April 2021

Abstract: A numerical study of heat transfer problem by natural convection of a fluid inside a square cavity with two inner bodies is presented. This subject is of great interest in the engineering area, mainly in applications involving development of heat exchangers and cooling or heating systems of bodies by natural convection mechanism. Two cases have been studied. The inner bodies are square in case 1 and circular in case 2. In both cases, the bodies are solid and thermally conductive, the cavity lower and upper horizontal surfaces are isothermal with high temperature Th and low temperature Tc, respectively. Both vertical surfaces are adiabatic. A FORTRAN code using Finite Element Method (FEM) is developed to simulate the problem and solve the governing equations. The distributions of stream function, ψ, dimensionless temperature, θ, and vorticity, ω, are determined. Heat transfer is evaluated by analyzing the behavior of the average Nusselt number.

Keywords: Heat Transfer, Natural Convection, Square Cavity, Finite Element Method, Inner Body

1. Introduction

In present days, research on natural convection in cavities has been the topic of the many studies. Natural convection in open cavities and slots is encountered in many engineering applications, like solar thermal receivers, heat convection from extended surfaces in heat exchangers, and solar power collectors with insulated strips Cavities with a side opening and internal heat source are often seen in many electronic devices, where the openings facilitate the cooling of the interior components of the apparatus. Furthermore, the study of this case has relevancy in many other applications, among which may be cited: construction and operation of nuclear reactors, solar power collectors, energy storage systems, design and construction of indoor environments, and grain storage. Many studies are reported within the literature, where the behavior of fluids within the cavities was evaluated, a number of which are cited below. The natural convection in cavities induced by the difference in temperature between vertical (or horizontal) walls is a case widely studied [2–15]. In those studies, the authors evaluated the influence of the temperature gradient [2–5,7–12], partial opening and dispositions of the cavity [6,13,15] thermal properties. A numerical study on heat distribution and thermal mixing during steady laminar natural convective flow within fluid-saturated porous square cavities has been considered for three different cases: uniformly heated bottom wall, discrete heat sources on walls, and uniformly heated left and bottom walls in Kaluri et al. [10]. Deng and Chang [11] study numerically a two dimensional steady and laminar natural convection in an air-filled rectangular enclosure where the horizontal walls are thermally insulated and the vertical side walls have two spatially varying sinusoidal temperature distributions of different amplitudes and phases. Michalek [12] conducted experiments to measure the water flow inside a cubical cavity with isothermal vertical walls and adiabatic horizontal walls for values of Ra greater than 10^9.

The transition from stationary to non-stationary flow was below the theoretical value of the critical Rayleigh number. Bilgen and Oztop [13] performed a numerical study of heat transfer by natural convection in an inclined and partially open 2D cavity. A parametric study was conducted for values of Ra between 103 and 106, concluding that the value of Nusselt number was maximized for angles between 30_ and 60_ for low values of Ra, while at high values of Ra, the value of the Nusselt number was maximized for angles between 60 and 90. Kuznik et al. [14] used the Lattice–Boltzmann method with a non-uniform mesh for the simulation of natural convection in a square cavity.

The authors determined the Rayleigh numbers for the transition region between 10^3 and 10^9, and observed a good agreement with those reported in the literature. The same method was used by Mezrhab et al. [15], where the influence of the cavity inclination and the existence of an internal partition were evaluated. There was a maximum reduction in heat transfer for the range of Rayleigh numbers between 6×10^3 and $2\ 10^4$. Some study combine effect of radiation and natural convection in cavities differentially heated [16– 18]. When there is an internal heat source in cavities large changes in the internal flow characteristics occur. Studies on natural convection in cavities with internal heat source can be found in Kuznetsov and Sheremet [19], Nakhi and Chamkha [20], Oztop and Bilgen [21], Oztop and Abu-Nada [22], and Bazylak et al. [23], or with internal

baffles in Fontana et al. [24]. In many cases, the cavity presents a partial opening, which facilitates mass flow and therefore the cooling process [25–29]. Mariani and Silva [28] conducted a numerical study of the thermal and fluid dynamics behavior of air in partially open 2D enclosures based on two aspects of the radius, H/W= 1 and 2. The enclosure had an opening on the right wall and a small heat source located on the bottom or left wall, occupying three different positions. Numerical simulations were performed for Ra in the range of 10^3 and 10^6 and it was found that changes in this parameter have significant effects on the average and local Nusselt numbers (Nu) of the enclosures. Another study was conducted by Mariani and Coelho [29] to investigate steady heat transfer and flow phenomena of natural convection of air in enclosures, with three aspect ratios (H/W = 1, 2, and 4), within which there is a local heat source on the bottom wall at three different positions. A similar study was carried out by Kandaswamy et al. [30], where the influence of the position and the size of the heat source were evaluated. This study was conducted for Grashof numbers between 10^3 and 10^5. Hence, this study investigates natural convection in a partially open square cavity with an opening in the right wall of three different sizes H/4, H/2, and 3H/4, where H is the cavity height. The cavity was submitted to temperature differences between the left and right vertical walls and had an internal heat conduction source. The influence of the internal heat source at intensities of R = 400, 1000 and 2000, and external Rayleigh numbers of $10^3 \leq Ra \leq 10^5$, on the thermal and fluid dynamics of the air inside the cavity and the mass inflow rate at the opening, was investigated. In the current study, Finite Element Method has been used to convert the non-linear coupled partial differential equations for flow and temperature field into a matrix form of equations, which can be solved iteratively with the help of a computer code. The Galerkin Finite Element Method of three nodded triangular elements is used to divide the physical domain into smaller segments, which is a pre-requisite for finite element method. Numerical results are presented in terms of stream functions, isotherms, temperature profiles and Nusselt numbers.

This study investigates natural convection in a partially open square cavity with an opening in the right wall of three different sizes H/4, H/2, and 3H/4, where H is the cavity height. The cavity was submitted to temperature differences between the left and right vertical walls and had an internal heat conduction source. The influence of the internal heat source at intensities of R = 400, 1000 and 2000, and external Rayleigh numbers of $10^3 \leq Ra \leq 10^5$, on the thermal and fluid dynamics of the air inside the cavity and the mass inflow rate at the opening, was investigated. In the current study, Finite Element Method has been used to convert the non-linear coupled partial differential equations for flow and temperature field into a matrix form of equations, which can be solved iteratively with the help of a computer code. The Galerkin Finite Element Method of three nodded triangular elements is used to divide the physical domain into smaller segments, which is a pre-requisite for finite element method. Numerical results are presented in terms temperature profiles and Nusselt number.

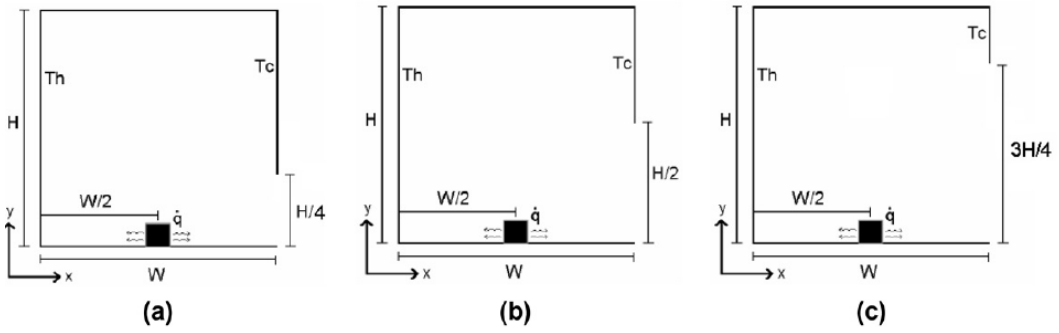

Fig. 1 shows a schematic diagram of the problem under consideration and the coordinate system. The system to be considered is a two-dimensional square cavity of width W and height H, where the two vertical walls are kept at different temperatures, T_h (left wall) and T_c (right wall), $T_h > T_c$. Zero heat flow is assumed at the top and bottom walls. The walls are rigid and no-slip conditions are imposed at the boundaries. The internal heat source is placed on the bottom horizontal wall, midway between the vertical walls, occupying 1% of the total volume of the cavity. The opening is placed on the right vertical wall of the cavity being evaluated for three conditions H⁄ = H/4, H/2, and 3H/4. The flow field is considered to be steady and the fluid is incompressible. Thermo physical properties of the fluid are assumed constant, with the exception of the density variation in the buoyancy term, i.e., the Boussinesq approximation is valid. The equations for the conservation of momentum and energy are

$$\frac{\partial u}{\partial x}+\frac{\partial v}{\partial y}=0 \tag{1.1}$$

$$u\frac{\partial v}{\partial x}+v\frac{\partial v}{\partial y}=-\frac{1}{\rho}\frac{\partial p}{\partial y}+\vartheta\left(\frac{\partial^2 v}{\partial x^2}+\frac{\partial^2 v}{\partial y^2}\right)+g\beta(T-T_c) \tag{1.2}$$

$$u\frac{\partial T}{\partial x}+v\frac{\partial T}{\partial y}=\alpha\left(\frac{\partial^2 T}{\partial x^2}+\frac{\partial^2 T}{\partial y^2}\right) \tag{1.3}$$

with boundary conditions

u (x , 0) = u(x, H) =u(0 , y) = u(H , y) = 0,

v (x , 0) = v(x, H) = v(0 , y) = v(H , y) = 0,

T (x, 0) = T_h ,

$$\frac{\partial T}{\partial y}(x,H)=0,\quad T(0,y)=T_h-(T_h-T_c)\frac{y}{H},$$

$$T(H,y)=T_h-(T_h-T_c)\frac{y}{H},\quad \frac{\partial T}{\partial y}(x,H)=0,\ 0<x<H$$

The Continuity equation (3.1) can be satisfied automatically by introducing the stream function 'ψ' as

$$u=\frac{\partial \psi}{\partial y} \tag{1.4a}$$

$$v=-\frac{\partial \psi}{\partial x} \tag{1.4b}$$

where x and y are the distances measured along the horizontal and vertical directions respectively u and v are the velocity components in the x and y directions respectively T denotes the temperature ϑ and α are kinematic viscosity and thermal diffusivity respectively K is the medium permeability P is the pressure and ρ is the density T_h and T_c are the temperatures at hot bottom wall and cold vertical wall respectively L is the side of the square cavity.

Using the following non dimensional variables,

Width $$X=\frac{x}{H}$$

Height $$Y=\frac{y}{H}$$

Velocity components $$\begin{cases}U=\dfrac{uH}{\alpha}\\ V=\dfrac{vH}{\alpha}\end{cases}$$

Stream function $$\overline{\psi}=\frac{\psi}{\alpha}$$

Pressure $$P=\frac{pH^2}{\rho\alpha^2}$$

Prandtl Number $$\mathrm{Pr}=\frac{\nu}{\alpha}$$

Rayleigh number $$Ra=\frac{g\beta(T_h-T_c)H^3\,\mathrm{Pr}}{\nu^2}$$

Temperature $$\theta=\frac{T-T_c}{T_h-T_c}$$

The governing equations (3.1)-(3.3) reduce to non-dimensional form as

$$\frac{\partial U}{\partial X}+\frac{\partial V}{\partial Y}=0 \tag{1.5}$$

$$U\frac{\partial V}{\partial X}+V\frac{\partial V}{\partial Y}=-\frac{\partial P}{\partial Y}+\Pr\left(\frac{\partial^2 V}{\partial X^2}+\frac{\partial^2 V}{\partial Y^2}\right)+Ra\,\Pr\theta \tag{1.6}$$

$$U\frac{\partial \theta}{\partial X}+V\frac{\partial \theta}{\partial Y}=\left(\frac{\partial^2 \theta}{\partial X^2}+\frac{\partial^2 \theta}{\partial Y^2}\right) \tag{1.7}$$

with the non dimensionless boundary conditions are

U (X , 0) = U(X, 1) = U(0 , Y) = U(1 ,Y) = 0,

V (X , 0) = V(X, 1) = V(0 , Y) = V(1, Y) = 0,

θ (X, 0) =1, $\frac{\partial \theta}{\partial Y}(X,1)=0, \quad \theta(0,Y)=\theta(1,Y)=1-Y$

where X and Y are dimensionless coordinates varying along horizontal and vertical directions respectively U and V are dimensionless velocity components in the X and Y directions respectively θ is the dimensionless temperature P is the dimensionless pressure Ra and Pr are Rayleigh Prandtl numbers respectively.

1.3. SOLUTION OF PROBLEM:

Thus far we have derived the partial differential equations, which describe the heat and fluid flow behavior in the vicinity of porous medium. The development of governing equations is one part but the second and important part is to solve these equations in order to predict the various parameters of interest in the porous medium. There are various numerical methods available to achieve the solution of these equations, but the most popular numerical methods are Finite difference method, Finite volume method and the Finite element method. The selection of these numerical methods is an important decision, which is influenced by variety of factors amongst which the geometry of domain plays a vital role. Other factors include the ease with which these partial differential equations can be transformed into simple forms, the computational time required and the flexibility in development of computer code to solve these equations.In the present study, we have predominantly used Finite Element Method (FEM). The following sections enlighten the Finite element method and present its application to solve the above-mentioned equations.

The Finite Element Method is a deservingly popular method amongst scientific community. This method was originally developed to study the mechanical stresses in a complex airframe structure popularized by Zienkiewicz and Cheung (23) by applying it to continuum mechanics. Since then the application of Finite Element Method has been exploited to solve the numerous problems in various engineering disciplines. The great thing about finite element method is its ease with which it can be generalized to myriad engineering problems comprised of different materials.

Another admirable feature of the Finite Element Method (FEM) is that it can be applied wide range of geometries having irregular boundaries, which is highly difficult to achieve with other contemporary methods. FEM can be said to have comprised of roughly 5 steps to solve any particular problem. The steps can be summarized as

- **Descritizing the domain:** This step involves the division of whole physical domain into smaller segments known as elements, and then identifying the nodes, coordinates of each node and ensuring proper connectivity between the nodes.
- **Specifying the equation:** In this step, the governing equation is specified and an equation is written in terms of nodal values
- **Development of Global matrix:** The equations are arranged in a global matrix which takes into account the whole domain
- **Solution:** The equations are solved to get the desired variable at each table in the domain
- **Evaluate the quantities of interest:** After solving the equations a set of values is obtained for each node, which can be further processed to get the quantities of interest.

There are varieties of elements available in FEM, which are distinguished by the presence of number of nodes. The present study is carried out by using a simple 3-noded triangular element as shown in fig. 2

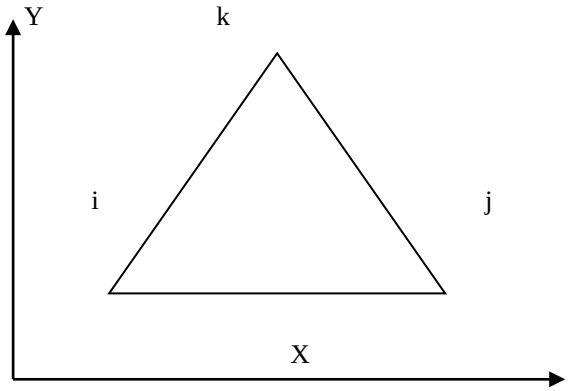

Fig.2:Typicaltriangular

Let us consider that the variable to be determined in the triangular area is 'θ'. The polynomial function for 'θ' can be expressed as:

$$\theta = \alpha_1 + \alpha_2 x + \alpha_3 y \quad (1)$$

The variable θ has the value θ_i, θ_j and θ_k at the nodal position i, j, and k of the element. The x and y coordinates at these points are x_i, x_j, x_k and y_i, y_j and y_k respectively. Substitution of these nodal values in the equation (1) helps in determining the constants α_1, α_2, α_3 which are:

$\alpha_1 = {}^1/_{2A} [(x_j y_k - x_k y_j) \theta_i + (x_k y_i - x_i y_k) \theta_j + (x_i y_j - x_j y_i) \theta_k]$ (2)

$\alpha_2 = {}^1/_{2A} [(y_j - y_k) \theta_i + (y_k - y_i) \theta_j + (y_i - y_j) \theta_k]$ (3)

$\alpha_3 = {}^1/_{2A} [(x_k - x_j) \theta_i + (x_i - x_k) \theta_j + (x_j - x_i) \theta_k]$ (4)

where A is area of the triangle given as

$$2A = \begin{vmatrix} 1 & x_i & y_i \\ 1 & x_j & y_j \\ 1 & x_k & y_k \end{vmatrix} \quad (5)$$

Substitution of α_1, α_2, α_3 in the equation (1) and mathematical arrangement of the terms results into

$$\theta = N_i \theta_i + N_j \theta_j + N_k \theta_k \quad (6)$$

In equation (6), N_i, N_j and N_k are the shape function given by

$$N_m = \frac{a_m + b_m x + c_m y}{2A}, \quad m = i, j, k \quad (7)$$

The constants can be expressed in terms of coordinates as

$a_i = x_j y_k - x_k y_j$
$b_i = y_j - y_k$ (8a)
$c_i = x_k - x_j$

$a_j = x_k y_i - x_i y_k$
$b_j = y_k - y_i$ (8b)
$c_j = x_i - x_k$

$a_k = x_i y_j - x_j y_i$
$b_k = y_i - y_j$ (8c)
$c_k = x_j - x_i$

The triangular element can be subdivided into three triangles with a point in the center of original triangle as shown in fig.3.

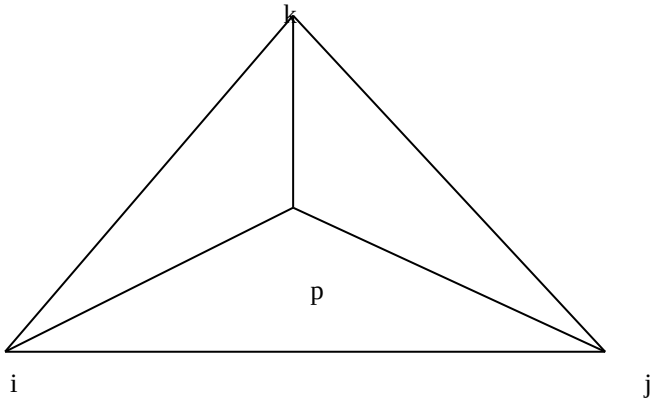

Fig.3: showing the sub triangular areas

Defining the new area ratios as

$$L_1 = \frac{area\ \ pij}{area\ \ ijk} \tag{9a}$$

$$L_2 = \frac{area\ \ pjk}{area\ \ ijk} \tag{9b}$$

$$L_3 = \frac{area\ \ pki}{area\ \ ijk} \tag{9c}$$

It can be shown that

$$L_1 = N_1 \tag{10a}$$

$$L_2 = N_2 \tag{10b}$$

$$L_3 = N_3 \tag{10c}$$

Good insight into the FEM is given in Segerlind [24], Galerkin method is employed to convert the partial differential equations into matrix form for an element. The steps invented are as given below. Please note that the nodal terms *i, j & k* are replaced by 1,2 & 3 respectively in subsequent discussions for simplicity.

The momentum and energy balance equations are solved using the Galerkin finite element method. Continuity equation will be used as a constraint due to mass conservation and this constraint may be used to obtain the pressure distribution. In order to solve equations, we use the finite element method where the pressure P is eliminated by a penalty parameter γ and the incompressibility criteria given by equation (3.5) which results in

$$P = -\gamma\left(\frac{\partial U}{\partial X} + \frac{\partial V}{\partial Y}\right) \tag{1.8}$$

The continuity equation (3.5) is automatically satisfied for large values of γ.

Using equation (3.8) and introducing stream function, the momentum equation (3.6) reduce to

$$U\frac{\partial V}{\partial X} + V\frac{\partial V}{\partial Y} = \gamma\frac{\partial}{\partial Y}\left(\frac{\partial U}{\partial X} + \frac{\partial V}{\partial Y}\right) + \Pr\left(\frac{\partial^2 V}{\partial X^2} + \frac{\partial^2 V}{\partial Y^2}\right) + Ra\,\Pr\theta \tag{1.9}$$

Finally momentum equation put in the form

$$\left[\frac{\partial\overline{\psi}}{\partial Y}\frac{\partial^2\overline{\psi}}{\partial X\partial Y} - \frac{\partial\overline{\psi}}{\partial X}\frac{\partial^2\overline{\psi}}{\partial Y^2}\right] = \gamma\left(\frac{\partial^2\overline{\psi}}{\partial Y^2}\frac{\partial\overline{\psi}}{\partial X} + \frac{\partial^2\overline{\psi}}{\partial Y^2}\right) + \Pr\left[\frac{\partial^2\overline{\psi}}{\partial X^2} + \frac{\partial^2\overline{\psi}}{\partial Y^2}\right] - Ra\,\Pr\theta \tag{1.10}$$

Application of Galerkin method to equation (3.10) yields:

$$\left\{R^e\right\}=-\int_A N^T \begin{Bmatrix} \left[\dfrac{\partial\overline{\psi}}{\partial Y}\dfrac{\partial^2\overline{\psi}}{\partial X\partial Y}-\dfrac{\partial\overline{\psi}}{\partial X}\dfrac{\partial^2\overline{\psi}}{\partial Y^2}\right]-\gamma\left(\dfrac{\partial^2\overline{\psi}}{\partial Y^2}\dfrac{\partial\overline{\psi}}{\partial X}+\dfrac{\partial^2\overline{\psi}}{\partial Y^2}\right) \\ -\Pr\left[\dfrac{\partial^2\overline{\psi}}{\partial X^2}+\dfrac{\partial^2\overline{\psi}}{\partial Y^2}\right]+Ra\,\Pr\theta \end{Bmatrix} dXdY \tag{1.11}$$

where R^e is the residue.

Considering the terms individually

$$\int_A [N]^T \frac{\partial\overline{\psi}}{\partial Y}\frac{\partial^2\overline{\psi}}{\partial X\partial Y}dA=\frac{1}{4A}\begin{Bmatrix} c_1\overline{\psi}_1+c_2\overline{\psi}_2+c_3\overline{\psi}_3 \\ c_1\overline{\psi}_1+c_2\overline{\psi}_2+c_3\overline{\psi}_3 \\ c_1\overline{\psi}_1+c_2\overline{\psi}_2+c_3\overline{\psi}_3 \end{Bmatrix}\left[b_1,b_2,b_3\right] \tag{1.12}$$

$$\int_A [N^T]\frac{\partial\overline{\psi}}{\partial X}\frac{\partial^2\overline{\psi}}{\partial Y^2}dA=\frac{1}{12A}\begin{Bmatrix} b_1\overline{\psi}_1+b_2\overline{\psi}_2+b_3\overline{\psi}_3 \\ b_1\overline{\psi}_1+b_2\overline{\psi}_2+b_3\overline{\psi}_3 \\ b_1\overline{\psi}_1+b_2\overline{\psi}_2+b_3\overline{\psi}_3 \end{Bmatrix}\left[c_1,c_2,c_3\right] \tag{1.13}$$

$$\int_A [N^T]\gamma\frac{\partial^2\overline{\psi}}{\partial Y^2}\frac{\partial\overline{\psi}}{\partial X}dA=\frac{\gamma}{12A}\begin{Bmatrix} b_1\overline{\psi}_1+b_2\overline{\psi}_2+b_3\overline{\psi}_3 \\ b_1\overline{\psi}_1+b_2\overline{\psi}_2+b_3\overline{\psi}_3 \\ b_1\overline{\psi}_1+b_2\overline{\psi}_2+b_3\overline{\psi}_3 \end{Bmatrix}\left[c_1,c_2,c_3\right] \tag{1.14}$$

$$\int_A [N^T]\gamma\frac{\partial^2\overline{\psi}}{\partial Y^2}dA=-\frac{\gamma}{4A}\begin{bmatrix} b_1^2 & b_1b_2 & b_1b_3 \\ b_1b_2 & b_2^2 & b_2b_3 \\ b_1b_3 & b_2b_3 & b_3^2 \end{bmatrix}\begin{bmatrix}\theta_1\\ \theta_2\\ \theta_3\end{bmatrix} \tag{1.15}$$

$$\int_A [N^T]\Pr\frac{\partial^2\overline{\psi}}{\partial X^2}dA=-\frac{\Pr}{4A}\begin{bmatrix} c_1^2 & c_1c_2 & c_1c_3 \\ c_1c_2 & c_2^2 & c_2c_3 \\ c_1c_3 & c_2c_3 & c_3^2 \end{bmatrix}\begin{bmatrix}\theta_1\\ \theta_2\\ \theta_3\end{bmatrix}$$

$$\int_A [N^T]\Pr\frac{\partial^2\overline{\psi}}{\partial Y^2}dA=-\frac{\Pr}{4A}\begin{bmatrix} b_1^2 & b_1b_2 & b_1b_3 \\ b_1b_2 & b_2^2 & b_2b_3 \\ b_1b_3 & b_2b_3 & b_3^2 \end{bmatrix}\begin{bmatrix}\theta_1\\ \theta_2\\ \theta_3\end{bmatrix} \tag{1.16}$$

$$\int_A [N]^T RaP\,\theta dA=\frac{RaP}{12A}\begin{bmatrix}\theta_1\\ \theta_2\\ \theta_3\end{bmatrix} \tag{1.17}$$

Thus the whole equation (3.10) can be written in matrix form as

$$\frac{1}{4A}\begin{Bmatrix} c_1\overline{\psi}_1 + c_2\overline{\psi}_2 + c_3\overline{\psi}_3 \\ c_1\overline{\psi}_1 + c_2\overline{\psi}_2 + c_3\overline{\psi}_3 \\ c_1\overline{\psi}_1 + c_2\overline{\psi}_2 + c_3\overline{\psi}_3 \end{Bmatrix}\begin{bmatrix} b_1, b_2, b_3 \end{bmatrix} - \frac{1}{12A}\begin{Bmatrix} b_1\overline{\psi}_1 + b_2\overline{\psi}_2 + b_3\overline{\psi}_3 \\ b_1\overline{\psi}_1 + b_2\overline{\psi}_2 + b_3\overline{\psi}_3 \\ b_1\overline{\psi}_1 + b_2\overline{\psi}_2 + b_3\overline{\psi}_3 \end{Bmatrix}\begin{bmatrix} c_1, c_2, c_3 \end{bmatrix}$$

$$+\frac{\gamma}{12A}\begin{Bmatrix} b_1\overline{\psi}_1 + b_2\overline{\psi}_2 + b_3\overline{\psi}_3 \\ b_1\overline{\psi}_1 + b_2\overline{\psi}_2 + b_3\overline{\psi}_3 \\ b_1\overline{\psi}_1 + b_2\overline{\psi}_2 + b_3\overline{\psi}_3 \end{Bmatrix}\begin{bmatrix} c_1, c_2, c_3 \end{bmatrix} + \frac{\gamma}{4A}\begin{bmatrix} b_1^2 & b_1b_2 & b_1b_3 \\ b_1b_2 & b_2^2 & b_2b_3 \\ b_1b_3 & b_2b_3 & b_3^2 \end{bmatrix}\begin{bmatrix} \theta_1 \\ \theta_2 \\ \theta_3 \end{bmatrix}$$

$$-\frac{\Pr}{4A}\begin{bmatrix} c_1^2 & c_1c_2 & c_1c_3 \\ c_1c_2 & c_2^2 & c_2c_3 \\ c_1c_3 & c_2c_3 & c_3^2 \end{bmatrix}\begin{bmatrix} \theta_1 \\ \theta_2 \\ \theta_3 \end{bmatrix} + -\frac{\Pr}{4A}\begin{bmatrix} b_1^2 & b_1b_2 & b_1b_3 \\ b_1b_2 & b_2^2 & b_2b_3 \\ b_1b_3 & b_2b_3 & b_3^2 \end{bmatrix}\begin{bmatrix} \theta_1 \\ \theta_2 \\ \theta_3 \end{bmatrix} + \frac{RaP}{12A}\begin{bmatrix} \theta_1 \\ \theta_2 \\ \theta_3 \end{bmatrix} = 0$$

(1.18)

Introducing stream function, the energy equation (3.7) reduces as

$$\frac{\partial\overline{\psi}}{\partial Y}\frac{\partial\theta}{\partial X} + \frac{\partial\overline{\psi}}{\partial X}\frac{\partial\theta}{\partial Y} = \left(\frac{\partial^2\theta}{\partial X^2} + \frac{\partial^2\theta}{\partial Y^2}\right) \tag{1.19}$$

FEM of Energy Equation is

$$\left\{R^e\right\} = -\int_A [N]^T\left(\frac{\partial\overline{\psi}}{\partial Y}\frac{\partial\theta}{\partial X} + \frac{\partial\overline{\psi}}{\partial X}\frac{\partial\theta}{\partial Y} - \frac{\partial^2\theta}{\partial X^2} - \frac{\partial^2\theta}{\partial Y^2}\right)dA \tag{1.20}$$

Considering the terms individually

$$\int_A [N]^T\frac{\partial\overline{\psi}}{\partial Y}\frac{\partial\overline{\theta}}{\partial X}dA = \frac{1}{12A}\begin{Bmatrix} c_1\overline{\psi}_1 + c_2\overline{\psi}_2 + c_3\overline{\psi}_3 \\ c_1\overline{\psi}_1 + c_2\overline{\psi}_2 + c_3\overline{\psi}_3 \\ c_1\overline{\psi}_1 + c_2\overline{\psi}_2 + c_3\overline{\psi}_3 \end{Bmatrix}\begin{bmatrix} b_1, b_2, b_3 \end{bmatrix}\begin{bmatrix} \theta_1 \\ \theta_2 \\ \theta_3 \end{bmatrix} \tag{1.21}$$

$$\int_A [N^T]\frac{\partial\overline{\psi}}{\partial X}\frac{\partial\theta}{\partial Y}dA = \frac{1}{12A}\begin{Bmatrix} b_1\overline{\psi}_1 + b_2\overline{\psi}_2 + b_3\overline{\psi}_3 \\ b_1\overline{\psi}_1 + b_2\overline{\psi}_2 + b_3\overline{\psi}_3 \\ b_1\overline{\psi}_1 + b_2\overline{\psi}_2 + b_3\overline{\psi}_3 \end{Bmatrix}\begin{bmatrix} c_1, c_2, c_3 \end{bmatrix}\begin{bmatrix} \theta_1 \\ \theta_2 \\ \theta_3 \end{bmatrix} \tag{1.22}$$

$$\int_A [N^T]\frac{\partial^2\theta}{\partial X^2}dA = -\frac{1}{4A}\begin{bmatrix} b_1^2 & b_1b_2 & b_1b_3 \\ b_1b_2 & b_2^2 & b_2b_3 \\ b_1b_3 & b_2b_3 & b_3^2 \end{bmatrix}\begin{bmatrix} \theta_1 \\ \theta_2 \\ \theta_3 \end{bmatrix} \tag{1.23}$$

$$\int_A [N^T]\frac{\partial^2\theta}{\partial Y^2}dA = -\frac{1}{4A}\begin{bmatrix} c_1^2 & c_1c_2 & c_1c_3 \\ c_1c_2 & c_2^2 & c_2c_3 \\ c_1c_3 & c_2c_3 & c_3^2 \end{bmatrix}\begin{bmatrix} \theta_1 \\ \theta_2 \\ \theta_3 \end{bmatrix} \tag{1.24}$$

Thus the whole equation (3.19) can be written in matrix form as

$$\frac{1}{12A}\begin{Bmatrix} c_1\overline{\psi}_1 + c_2\overline{\psi}_2 + c_3\overline{\psi}_3 \\ c_1\overline{\psi}_1 + c_2\overline{\psi}_2 + c_3\overline{\psi}_3 \\ c_1\overline{\psi}_1 + c_2\overline{\psi}_2 + c_3\overline{\psi}_3 \end{Bmatrix} [b_1, b_2, b_3] \begin{bmatrix} \theta_1 \\ \theta_2 \\ \theta_3 \end{bmatrix} - \frac{1}{12A}\begin{Bmatrix} b_1\overline{\psi}_1 + b_2\overline{\psi}_2 + b_3\overline{\psi}_3 \\ b_1\overline{\psi}_1 + b_2\overline{\psi}_2 + b_3\overline{\psi}_3 \\ b_1\overline{\psi}_1 + b_2\overline{\psi}_2 + b_3\overline{\psi}_3 \end{Bmatrix} [c_1, c_2, c_3] \begin{bmatrix} \theta_1 \\ \theta_2 \\ \theta_3 \end{bmatrix}$$

$$-\frac{1}{4A}\begin{bmatrix} b_1^2 & b_1b_2 & b_1b_3 \\ b_1b_2 & b_2^2 & b_2b_3 \\ b_1b_3 & b_2b_3 & b_3^2 \end{bmatrix} \begin{bmatrix} \theta_1 \\ \theta_2 \\ \theta_3 \end{bmatrix} + \frac{1}{4A}\begin{bmatrix} c_1^2 & c_1c_2 & c_1c_3 \\ c_1c_2 & c_2^2 & c_2c_3 \\ c_1c_3 & c_2c_3 & c_3^2 \end{bmatrix} \begin{bmatrix} \theta_1 \\ \theta_2 \\ \theta_3 \end{bmatrix} = 0 \qquad (1.25)$$

1.4. NUSSLET NUMBER:

The average dimensionless Nusselt Number ($\overline{Nu}$) can be evaluated using the formula

$$\overline{Nu} = -\frac{\partial\theta}{\partial n} \qquad (1.26)$$

where n denotes the normal direction on a plane.

The average Nusselt numbers at bottom wall ($\overline{Nu}_b$) and at the side wall ($\overline{Nu}_s$) are defined as

$$\overline{Nu}_b = \int_0^1 Nu_b dX \qquad (1.27)$$

$$\overline{Nu}_s = \int_0^1 Nu_s dY \qquad (1.28)$$

1.5. RESULTS AND DISCUSSION:

The computational domain consists of 20 × 20 bi-quadratic elements which correspond to 41 × 41 grid points. The bi-quadratic elements with lesser number of nodes smoothly capture the non-linear variations of the field variables which are in contrast with finite element method solutions available. Figs. 4 – 9 illustrate the stream function and isotherm contours for various values of Ra = 10^3–10^5 and Pr = 0.7–10 with uniformly heated bottom wall and linearly heated side walls where the top wall is well insulated. As expected due to the linearly heated vertical walls and the uniformly heated bottom wall, fluids rise up from the middle portion of the bottom wall and flow down along two vertical walls forming two symmetric rolls with clockwise and anti-clockwise rotations inside the cavity. At Ra = 10^3, the magnitudes of stream functions are considerably lower and the heat transfer is due to purely conduction. During conduction dominant heat transfer the temperature $\theta \leq$ 0.3 occur symmetrically near the side walls of the enclosure. The other temperature contours with $\theta \geq 0.4$ are smooth curves which span the entire enclosure and they are generally symmetric with respect to the vertical symmetric line. The temperature contours as indicated in Fig. 4 remains invariant up to Ra < 10^4. At Ra = 10^4, the circulation near the central regimes are stronger and consequently, the temperature contour with θ = 0.5 starts getting shifted towards the side wall and break into two symmetric contour lines (Fig.5) The presence of significant convection is also exhibited in Fig. 6 at Ra = 10^4 where temperature contour for θ = 0.6 starts getting deformed and pushed towards the top plate. In addition, it may be noted that the secondary circulations appear at the bottom corners for Ra = 10^4 due to convection as the lower half of the vertical walls are hot and the hot fluids move towards the center of the cavity. Consequently at Ra = 10^4 the stronger secondary circulations enhance the mixing process which result in the rejoining of temperature contour θ = 0.6 (Fig. 7). Further at Ra = 10^5 the primary circulation pushed towards the upper part of the cavity and due to enhanced convection from the linear hot vertical wall, the isotherm lines with greater values θ > 0.5 covers almost 70% of the cavity (Fig. 8). It is interesting to observe that due to two pairs of symmetric circulations, 'hot' and 'cold' fluid regimes appear distinctly across the temperature contour θ = 0.6. In contrast at Ra = 10^5 for Pr = 10 the strength of secondary circulations appearing at corners of bottom wall is less as compared for Pr = 0.7 case due to the viscous force dominating the buoyancy force for Pr = 10 (Fig. 9). As the strength of the primary circulation increases for Pr = 10 case, the isotherm lines with temperature contours θ > 0.5 covers approximately 90% of cavity. The significant effect of convective heat transfer will be illustrated later via

average Nusslet number vs Rayleigh number plot. Figs. 10 –12 illustrate the stream function and isotherm contours for various values of Ra = 10^3–10^5 and Pr = 0.7 –10 with uniformly heated bottom wall, cooled right wall and the left wall is linearly heated. As expected, due to linearly heated left wall, fluids rise up along the side of left wall and flow down along the cooled right wall forming a roll with clockwise rotation inside the cavity. As Ra increase from 10^3 to 10^5, the value of stream function increases i.e., the flow rate increases. At the left corner of the top wall, secondary circulation formed due to convection and the hot fluids move towards the left corner of the cavity. Fig. 10 shows that the isotherm lines change its value smoothly from hot vertical wall to cold vertical wall for Ra = 10^3. At Ra = 10^4 the circulations are stronger and consequently the temperature contour with θ = 0.5 pushed towards the right corner of top wall (Fig. 11). At Ra = 10^5 in Fig. 12 due to enhanced convection from the hot left wall to the cold right wall, the isotherm lines with greater values θ > 0.5 covers around 50% of the cavity for Pr = 0.7 and Pr = 10. In addition for Pr = 10, the strength of secondary circulation increases. Fig. 13 and Fig. 14 display the effects of Ra and Pr on the local Nusselt numbers at the bottom and side walls (Nu_b, Nu_s) for linearly heated side walls. At the edges of the bottom wall the heat transfer rate Nu_b is 1 due to the linearly heated side walls (Fig. 13). For Ra = 10^4, the heat transfer rate is minimum value at the center of the bottom wall due to the higher values of stream function (i.e., flow rate) with two symmetric circulations about the vertical symmetric line at the center of the bottom wall. Heat transfer rate prevails at Ra = 10^5 and Pr = 10. In contrast for Ra = 10^5 and Pr = 0.7 the heat transfer rate is maximum at center of the bottom wall due to the presence of strong secondary circulations leading to a high temperature gradient at the center of the bottom wall. In Fig.14 the heat transfer rate at the bottom-edge of side wall is zero due to uniformly heated bottom wall and the heat transfer rate is maximum at the top-edge of side wall due to insulated top wall. For Ra = 10^3 and Pr = 0.7, due to weak circulations the heat transfer rate is almost zero upto Y = 0.7 and Nu_s = 3 at Y = 1 whereas at Ra = 10^4, the heat transfer rate Nu_s = 4 at Y = 1 due to stronger circulations. For Ra = 10^5, due to the presence of a pair of symmetric secondary circulated cells with clockwise and anti-clockwise rotations, the heat transfer rate is oscillatory in nature in the lower half of the side walls and the increasing trend of heat transfer rate is observed in the upper half of the side walls with Nu_s = 6 and Nu_s = 8 at Y = 1 corresponding to Pr = 0.7 and Pr = 10 respectively. The overall effects upon the heat transfer rates are displayed for linearly heated side walls in Fig. 15 and Fig.16, where the distributions of the average Nusselt number of bottom wall and side walls respectively are plotted vs the Rayleigh number. It is observed that the average Nusselt number is almost constant up to Ra = 10^4 due to dominant heat conduction mode and smoothly increases as Rayleigh number increases further. It is interesting to note that the smoothness breaks at Ra = 10^4 and Pr = 0.7 for both bottom and side walls as the oppositely rotated secondary cells becomes prominent. The smoothly increasing trend of average Nusselt numbers is observed for Pr = 10 due to insignificant secondary cells. Fig. 17 and Fig. 18 display the effects of Ra and Pr on local Nusselt numbers at the bottom and side walls (Nu_b, Nu_s) for linearly heated left wall and cooled right wall. The heat transfer rate Nu_b is 0 at the left-edge of the bottom wall due to the linearly heated left wall and it is maximum at the right-edge of the bottom wall due to the cooled right wall (Fig. 17). As Ra increases from 10^3 to 10^5, the heat transfer rate increases from the left edge to the right-edge of the bottom wall. In Fig. 18, the heat transfer rate at the bottom edge of the left wall is zero due to the uniformly heated bottom wall and linearly heated left wall and its magnitude increases from the bottom edge to the top edge of the left wall. At Ra = 10^5, local Nusselt number (exhibits oscillatory behavior due to the presence of secondary circulation near the top edge of the left wall. The inset plot shows the local Nusselt number distribution for the right wall. For all values of Ra and Pr it is observed that Nusselt number is maximum at the bottom edge and decreases towards the top edge.

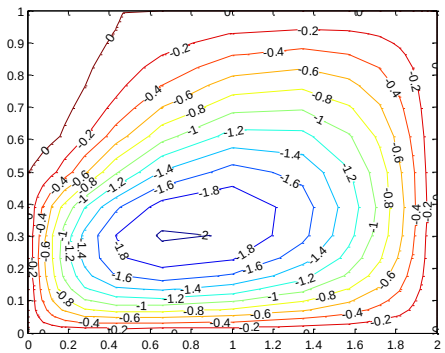

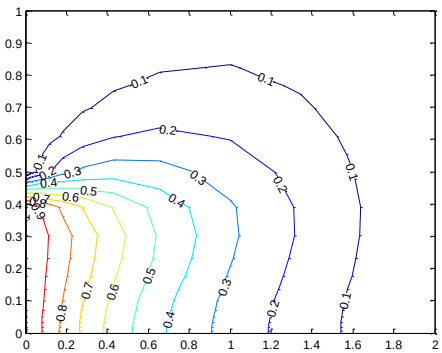

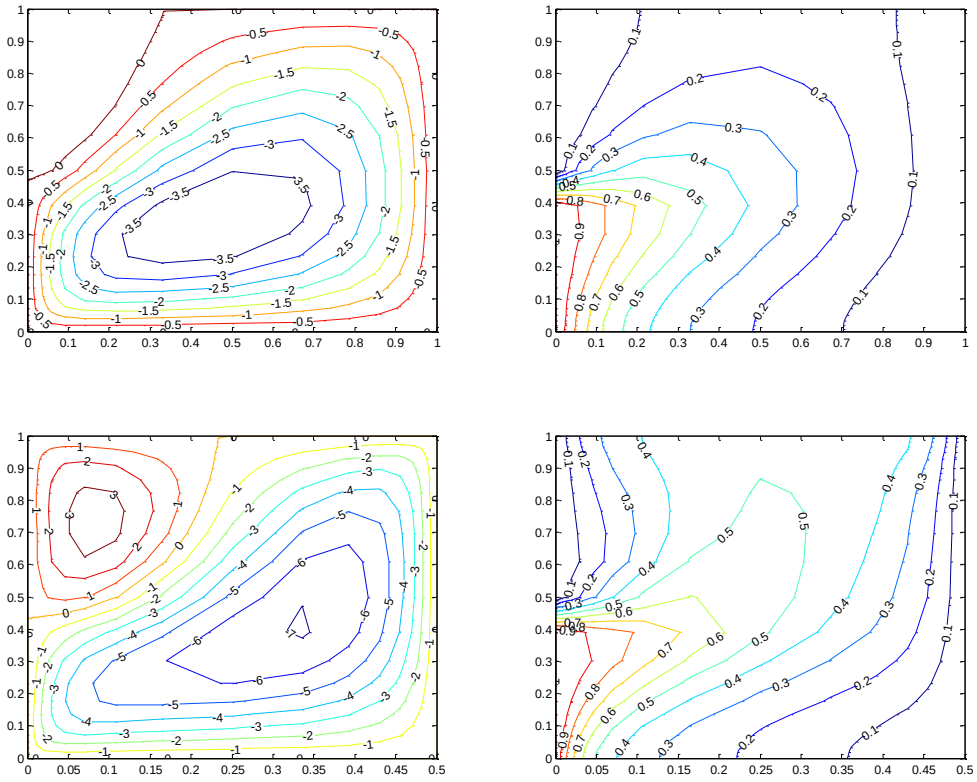

Fig. 4: Contour plots for linearly heated vertical walls, θ (0, Y) = θ (1, Y) = 1-Y with Pr = 0.7 and Ra = 10^3. Clockwise and anti-clockwise flows are shown via negative and positive signs of stream functions (Left) and Isotherms (Right) respectively.

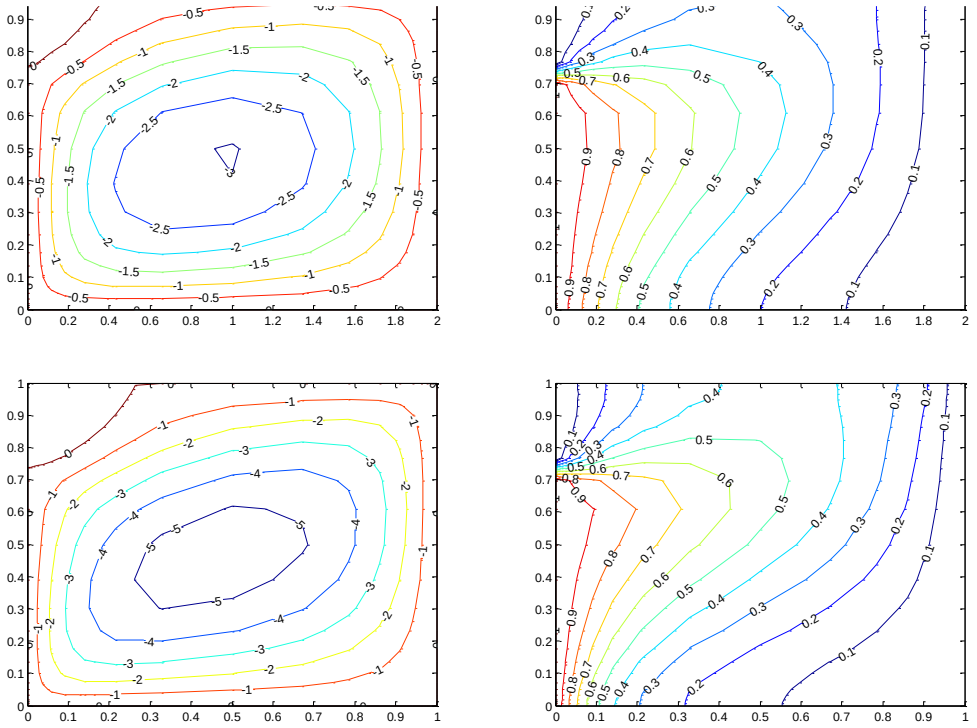

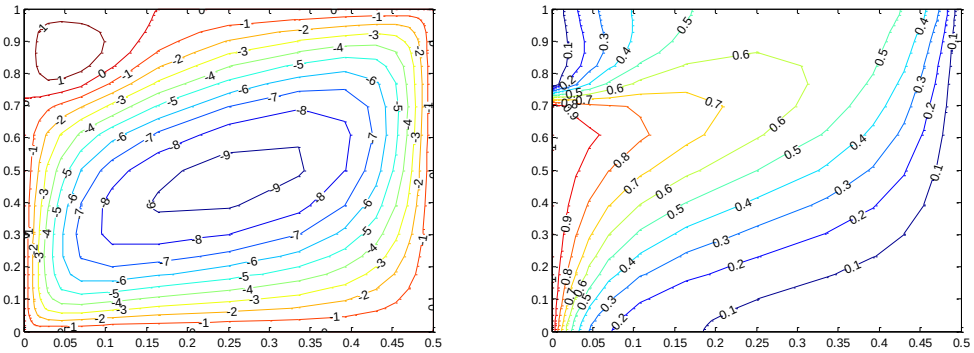

Fig. 5: Contour plots for linearly heated vertical walls, θ(0, Y) = θ(1, Y) = 1-Y with Pr = 0.7 and Ra = 10^4. Clockwise and anti-clockwise flows are shown via negative and positive signs of stream functions (Left) and Isotherms (Right) respectively.

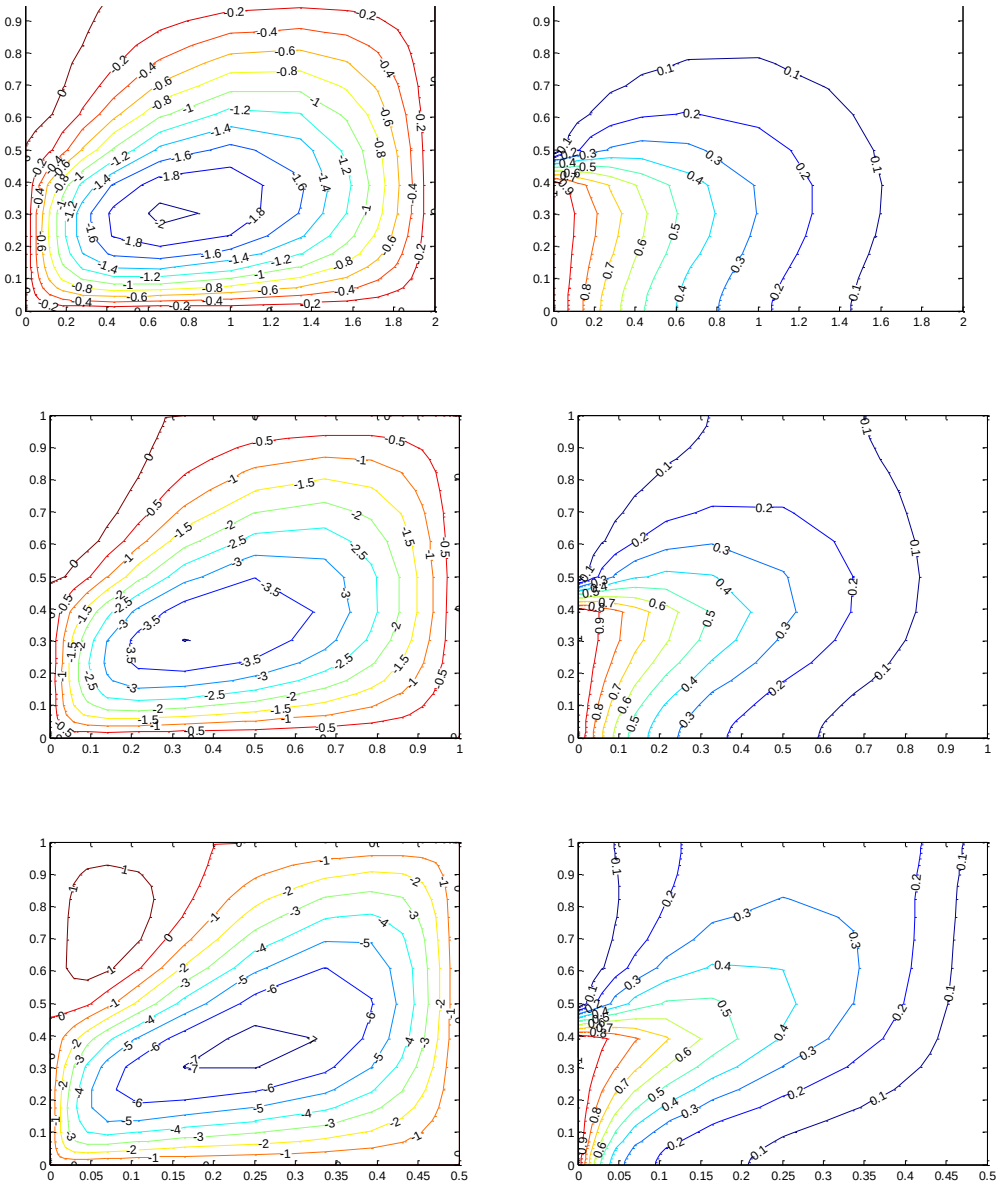

Fig. 6: Contour plots for linearly heated vertical walls θ(0, Y) = θ(1, Y) = 1-Y with Pr = 0.7 and Ra = 10^4. Clockwise and anti-clockwise flows are shown via negative and positive signs of stream functions (Left) and Isotherms (Right) respectively.

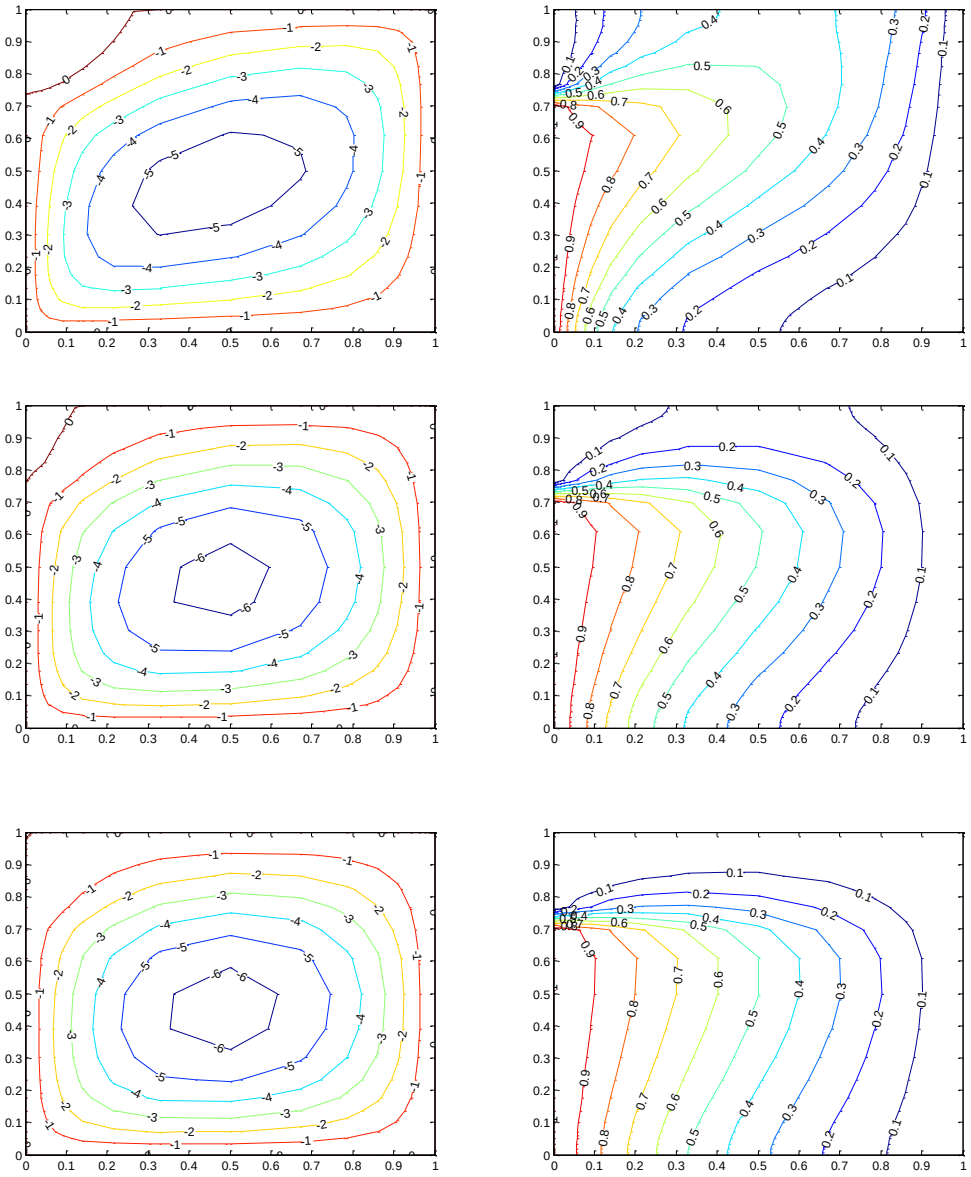

Fig. 7: Contour plots for linearly heated vertical walls, θ (0, Y) = θ (1, Y) = 1-Y with Pr = 0.7 and Ra = 10^4. Clockwise and anti-clockwise flows are shown via negative and positive signs of stream functions (Left) and Isotherms (Right) respectively.

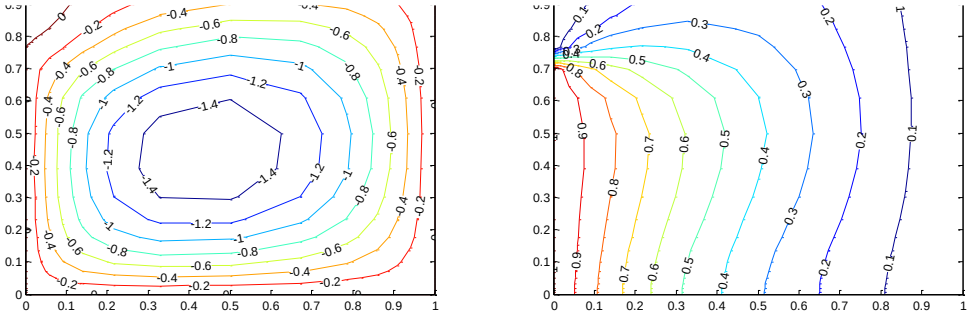

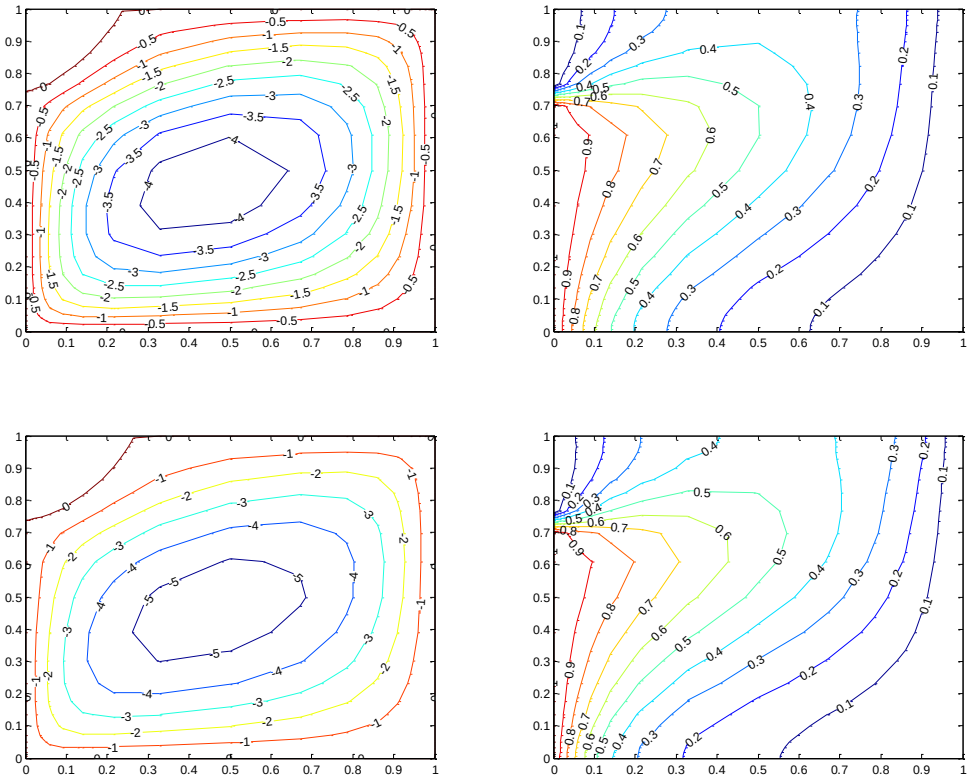

Fig. 8: Contour plots for linearly heated vertical walls, θ(0, Y) = θ(1, Y) = 1-Y with Pr = 0.7 and Ra = 10^5. Clockwise and anti-clockwise flows are shown via negative and positive signs of stream functions (Left) and Isotherms (Right) respectively.

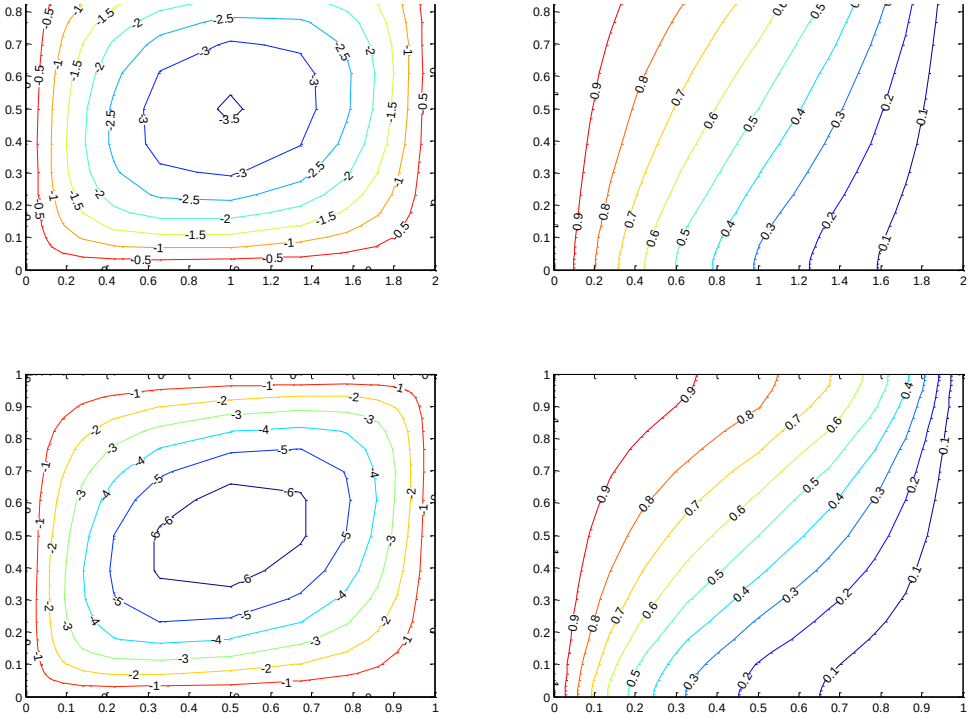

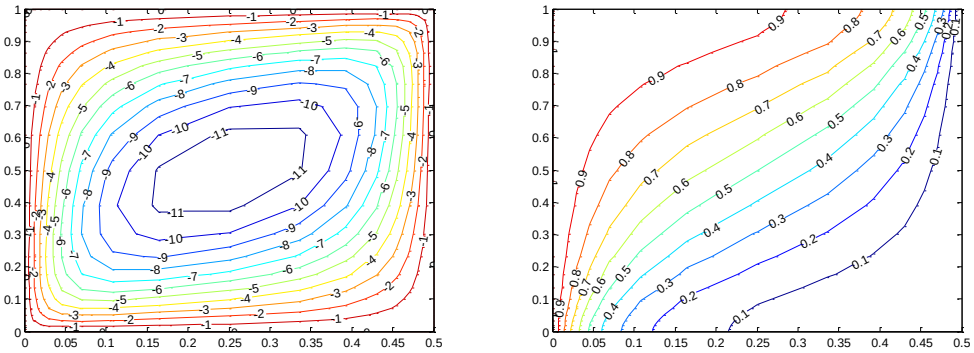

Fig 9: Contour plots for linearly heated vertical walls θ(0, Y) = θ(1, Y) = 1-Y with Pr = 10 and Ra = 10^5. Clockwise and anti-clockwise flows are shown via negative and positive signs of stream functions (Left) and Isotherms (Right) respectively.

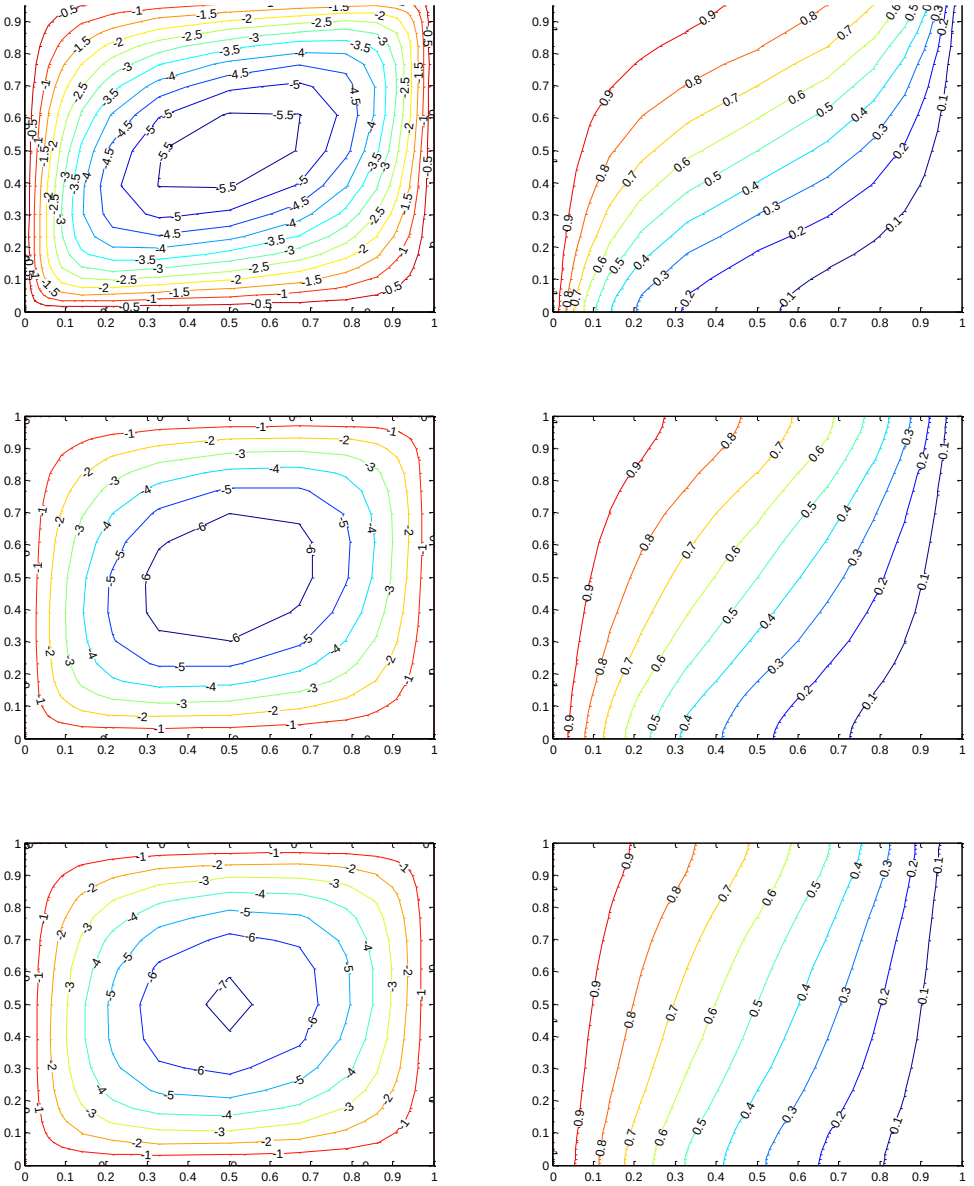

Fig 10: Contour plots for linearly heated vertical walls, θ(0, Y) = 1-Y, and cooled vertical wall θ(1,Y)=0 with Pr = 0.7 and Ra = 10^3. Clockwise and anti-clockwise flows are shown via negative and positive signs of stream functions (Left) and Isotherms (Right) respectively.

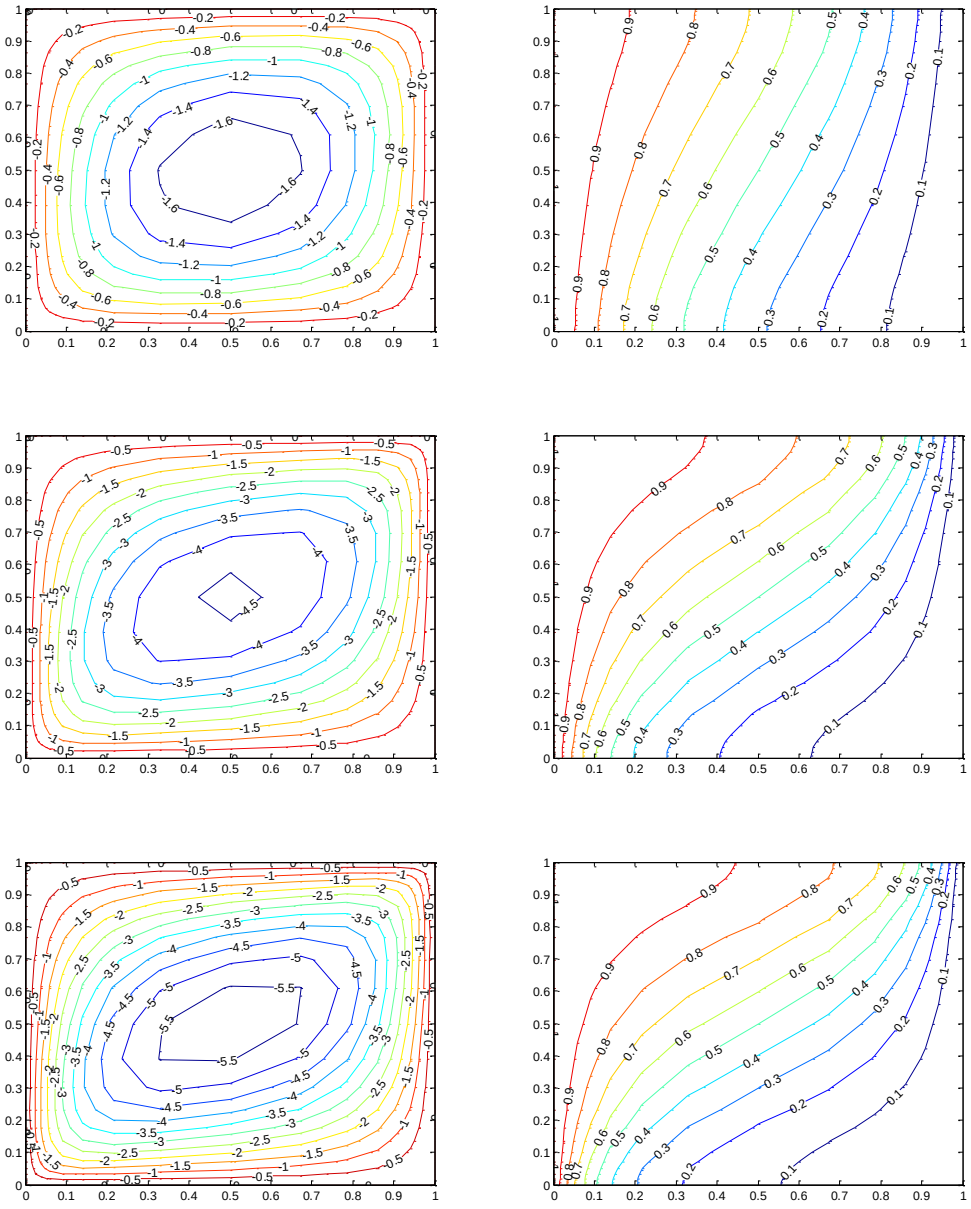

Fig. 11: Contour plots for linearly heated vertical walls, θ(0, Y) = 1-Y and cooled vertical wall θ(1, Y) =0 with Pr = 0.7 and Ra = 10^4. Clockwise and anti-clockwise flows are shown via negative and positive signs of stream functions (Left) and Isotherms (Right) respectively.

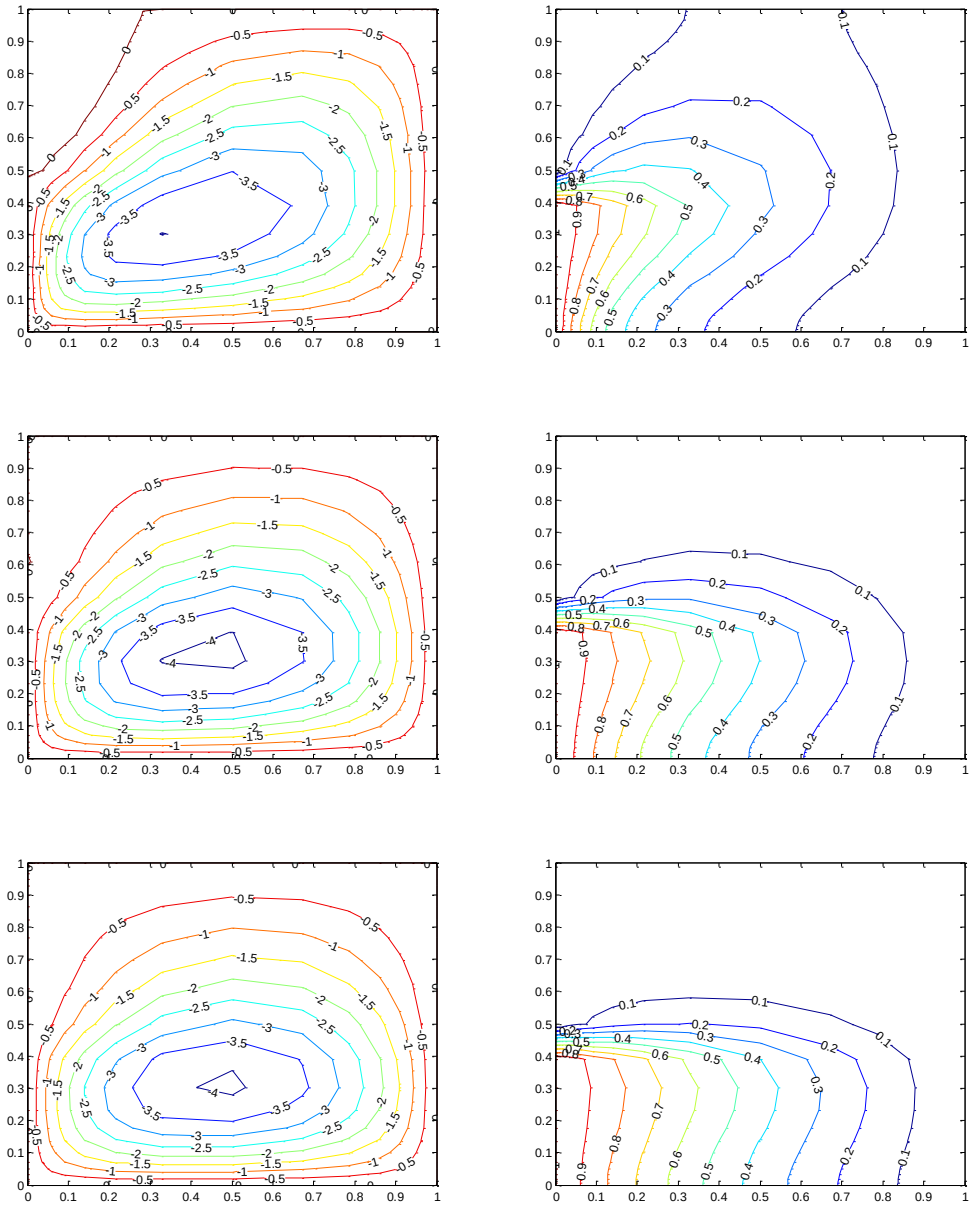

Fig. 12: Contour plots for linearly heated vertical walls θ(0, Y) = 1-Y and cooled vertical wall θ(1, Y) =0 with Pr = 10 and Ra = 10^5. Clockwise and anti-clockwise flows are shown via negative and positive signs of stream functions (Left) and Isotherms (Right) respectively.

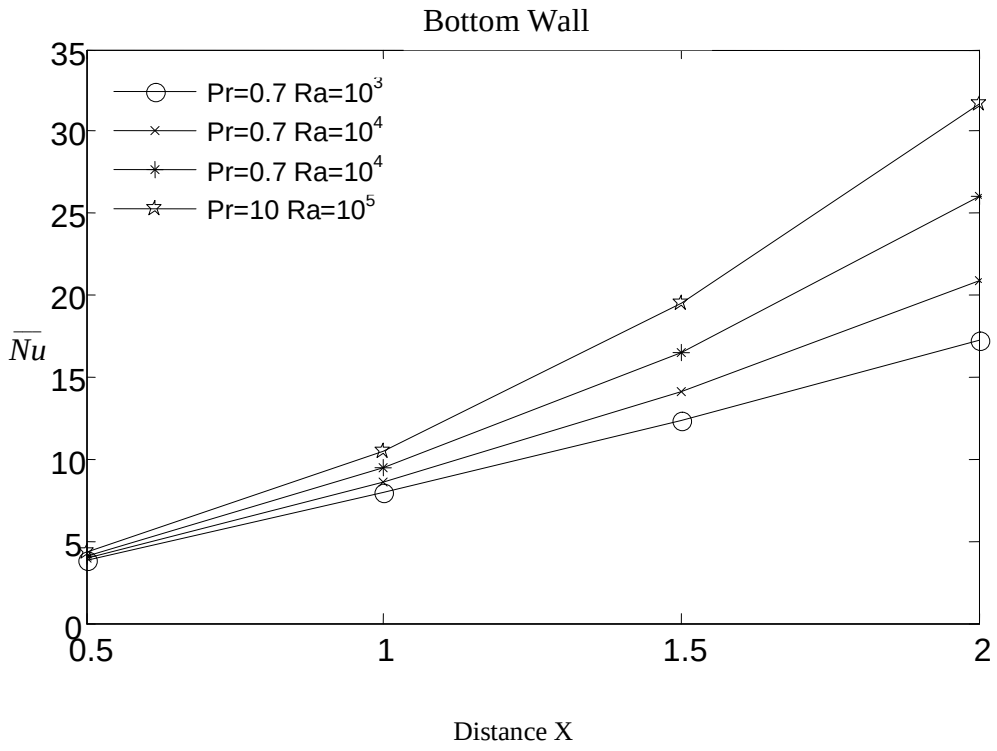

Fig.13: $\overline{Nu}$ Variations with distance at bottom wall for different values of Ra

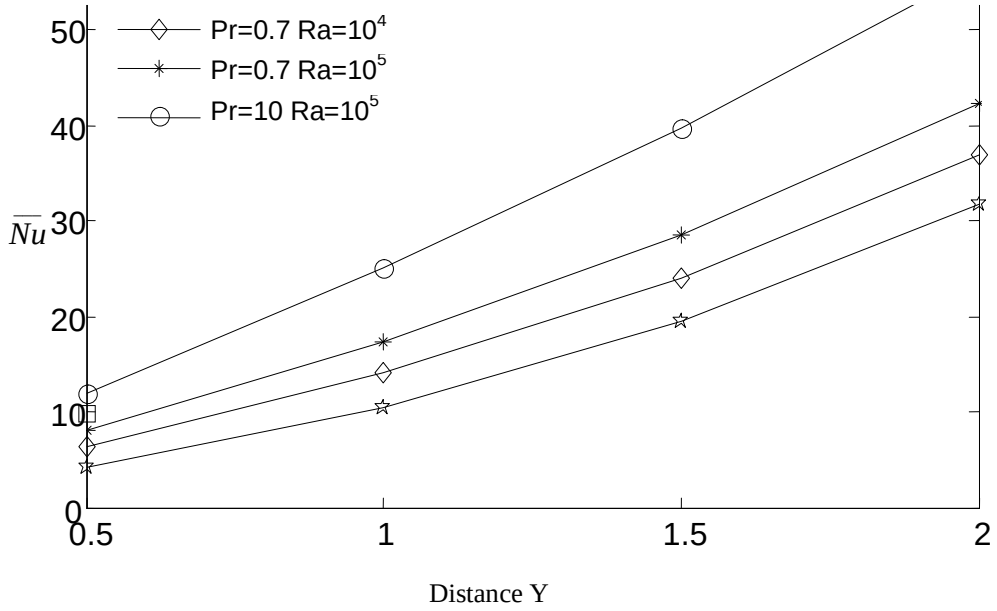

Fig. 14: $\overline{Nu}$ Variations with distance at side wall for linearly heated side wall for different values of Ra

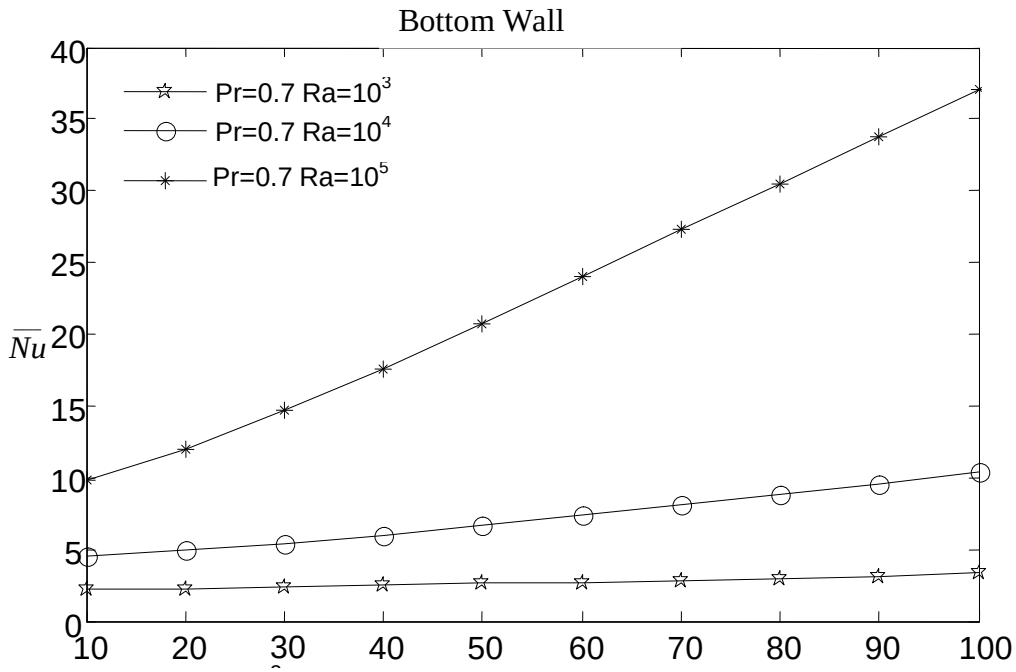

Fig. 15: $\overline{Nu}$ Variations with Rayleigh number for linearly heated side walls

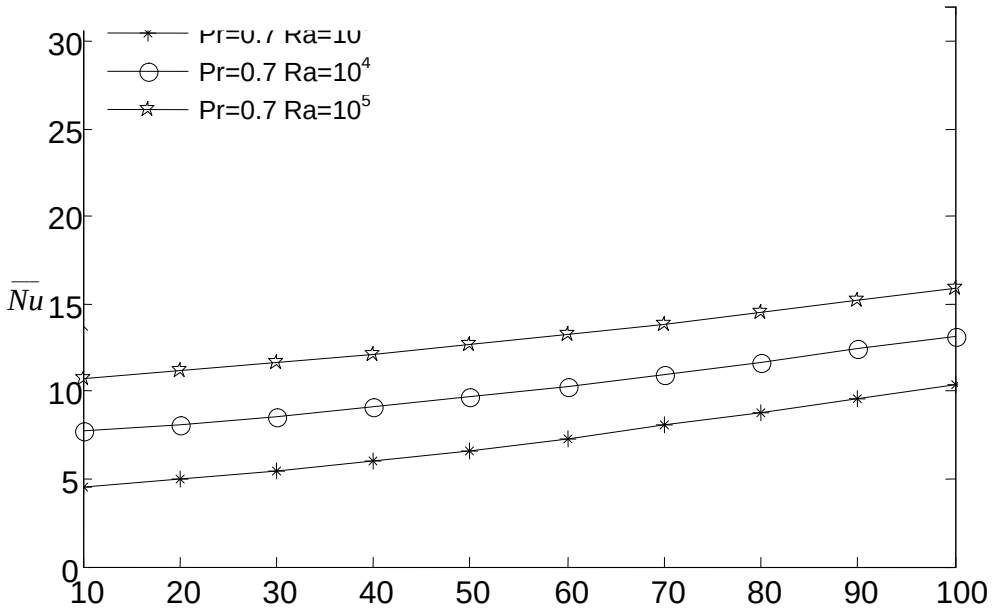

Fig.16: $\overline{Nu}$ Variations with Rayleigh number for linearly heated side walls

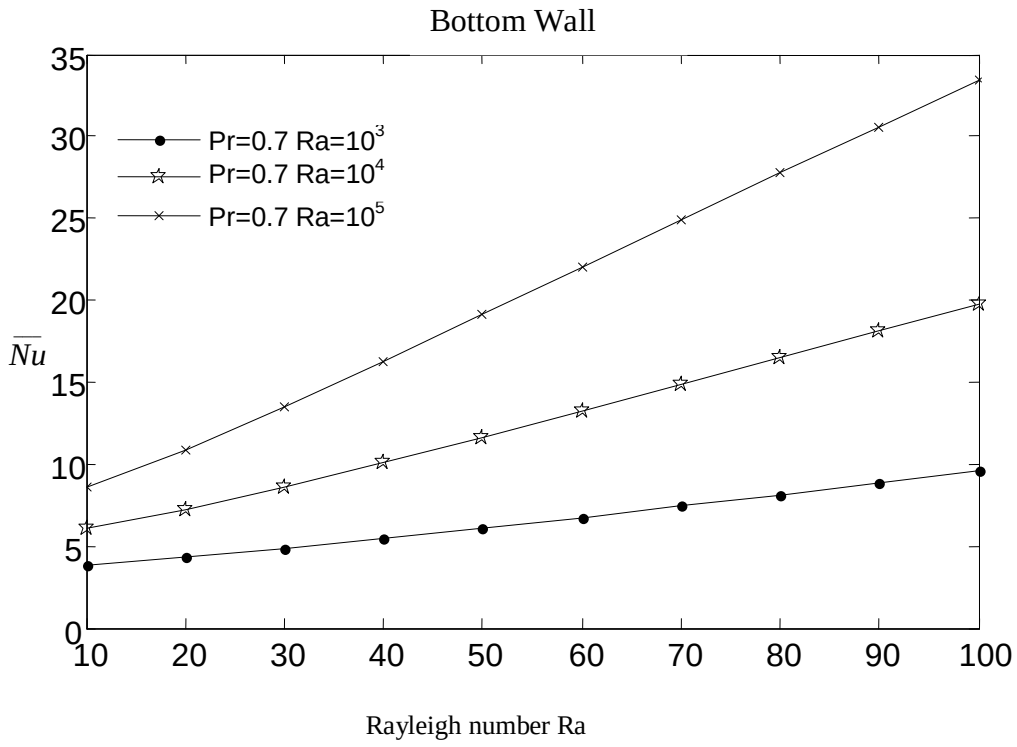

Fig.17: $\overline{Nu}$ Variations with Rayleigh number for linearly heated left wall

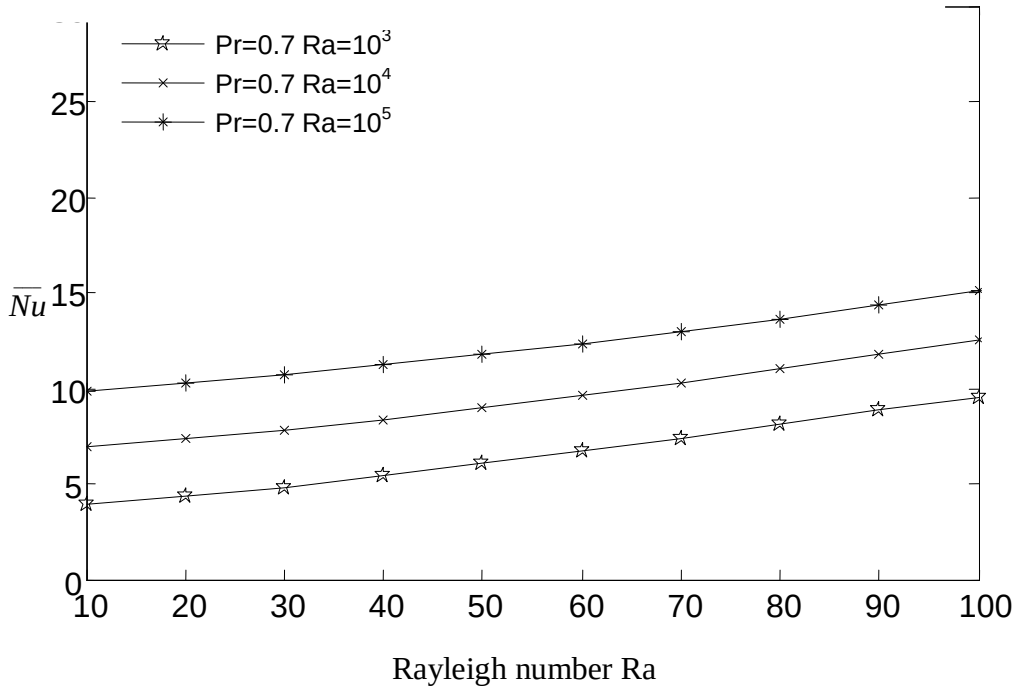

Fig.18: $\overline{Nu}$ Variations with Rayleigh number for linearly heated right wall

References

1. Sezai, A.A. Mohamad, Suppressing free convection from a flat plate with poor conductor ribs, Int. J. Heat Mass Transfer 42 (1998) 2041–2051.

2. T. Pesso, S. Piva, Laminar natural convection in a square cavity: low Prandtl numbers and large density differences, Int. J. Heat Mass Transfer 52 (2009).
3. T. Zitzmann, M.P. Cook, P. Pfrommer, S. Rees, L. Marjanovic, Simulation of steady state natural convection using CFD, in: Proceeding of Building Simulation, Montreal, Canada, 2005, pp. 1–8.
4. V.A.F. Costa, Thermodynamic of natural convection in enclosures with viscous dissipation, Int. J. Heat Mass Transfer 48 (2005) 2333–2341.
5. G.V. Davis, Natural convection of air in a square cavity: a bench mark numerical solution, Int. J. Numer. Methods Fluids 3 (2005) 249–264.
6. B. Abourida, M. Hasnaoui, S. Douamma, Natural convection in a square cavity with vertical boundaries submitted to periodic temperatures, Rev. Gen.
7. Therm. B.S. Yilbas, S.Z. Shuja, S.A. Gradebo, H.I. Al-Hamayel, K. Boran, Natural convection and entropy generation in a square cavity, Int. J. Energy Res.
8. G. Barakos, E. Mitsoulis, D. Assimacopoulos, Natural convection flow in a square cavity revisited: laminar and turbulent models with walls functions, Int. J. Numer. Methods Fluids 18 (2005) 695–719.
9. B.A.V. Bennett, J. Hsueh, Natural convection in a cubic cavity: implicit numerical solution of two benchmark problems, Numer. Heat Transfer A Appl.
10. R.S. Kaluri, T. Basak, S. Roy, Bejan's heatlines and numerical visualization of heat flow and thermal mixing in various differentially heated porous square cavities, Numer. Heat Transfer A Appl. 55 (2009) 487–516.
11. Q.H. Deng, J.J. Chang, Natural convection in a rectangular enclosure with sinusoidal temperature distributions on both side walls, Numer. Heat Transfer A Appl. 54 (2008) 507–524.
12. T. Michalek, High Rayleigh number natural convection in a cubic enclosure, in: Proceeding of Eurotherm Seminar of Numerical Heat Transfer, Gliwice- Cracow, Poland, 2005, pp. 1–11.
13. E. Bilgen, H. Oztop, Natural convection heat transfer in partially open inclined square cavities, Int. J. Heat Mass Transfer 48 (2005) 1470–1479.
14. F. Kuznik, J. Vareilles, G. Rusaouen, G. Krauss, A double-population lattice Boltzmann method with non-uniform mesh for the simulation of natural convection in a square cavity, Int. J. Heat Fluid Flow 28 (2007) 862–870.
15. Mezrhab, M. Jami, C. Abid, M. Bouzidi, P. Lallemand, Lattice–Boltzmann modelling of natural convection in an inclined square enclosure with partitions attached to its cold wall, Int. J. Heat Fluid Flow 27 (2006) 456–465.
16. Bahlaoui, A. Raji, R. El Ayachi, M. Hasnaoui, M. Lamsaadi, M. Naïmi, Coupled natural convection and radiation in a horizontal rectangular enclosure discretely heated from below, Numer. Heat Transfer A Appl. 52 (2007)1027–1042.
17. R. El Ayachi, A. Raji, M. Hasnaoui, A. Bahlaoui, Combined effect of radiation and natural convection in a square cavity differentially heated with a periodic temperature, Numer. Heat Transfer A Appl. 53 (2008) 1339–1356.
18. J.F. Hinojosa, C.A. Estrada, R.E. Cabanillas, G. Alvarez, Numerical study of transient and steady-state natural convection and surface thermal radiation in a horizontal square open cavity, Numer. Heat Transfer A Appl. 48 (2005) 179–196.
19. G.V. Kuznetsov, M.A. Sheremet, Conjugate heat transfer in an enclosure under the condition of internal mass transfer and in the presence of the local heat source, Int. J. Heat Mass Transfer 52 (2009) 1–8.
20. A.B. Nakhi, A.J. Chamkha, Conjugate natural convection around a finned pipe in a square enclosure with internal heat generation, Int. J. Heat Mass Transfer.
21. H. Oztop, E. Bilgen, Natural convection in differentially heated and partially divided square cavities with internal heat generation, Int. J. Heat Fluid Flow.
22. H.F. Oztop, E. Abu-Nada, Numerical study of natural convection in partially heated rectangular enclosures filled with nanofluids, Int. J. Heat Fluid Flow.
23. Bazylak, N. Djilali, D. Sinton, Natural convection in an enclosure with distributed heat sources, Numer. Heat Transfer A Appl. 49 (2006) 655–667.
24. É. Fontana, A. Silva, V.C. Mariani, F. Marcondes, The influence of baffles on the natural convection in trapezoidal cavities, Numer. Heat Transfer A Appl. 58 (2010) 125–145.
25. S. Sivasankaran, C.J. Ho, Buoyancy- and thermocapillary-induced convection of cold water in an open enclosure with variable fluid properties, Numer. Heat Transfer A Appl. 58 (2010) 457–474.
26. T.H. Hsu, K.Y. Hong, Natural convection of micropolar fluids in an open cavity, Numer. Heat Transfer A Appl. 50 (2006) 281–300.

27. A.Andreozzi, O. Manca, Numerical investigation on the steady state natural convection in a horizontal open-ended cavity with a heated upper wall, Numer. Heat Transfer A Appl. 57 (2010) 453–472.
28. V.C. Mariani, A. Silva, Natural convection: analysis of partially open enclosures with an internal heated source, Numer. Heat Transfer A Appl. 52 (2007) 595–619.
29. V.C. Mariani, L.S. Coelho, Partially open enclosures containing an internal local heat source, Braz. J. Chem. Eng. 24 (2007) 375–388.
30. P. Kandaswamy, J. Lee, A. Hakeem, Natural convection in a square cavity in the presence of heated plate, Nonlinear Anal. Model. Control 12 (2007) 203–212.
31. M. Hortmann, M. Peric, G. Scheuerer, Finite volume multigrid prediction of laminar natural convection: benchmark solutions, Int. J. Numer. Methods Fluids 11 (1990) 189–207.
32. J.L. Xia, Z.W. Zhou, Natural convection in an externally heated partially open cavity with a heated protrusion, FED-vol. 143/HTD, Measurement and Modeling of Environmental Flows – ASME, vol. 232, 1992, pp. 201–208